



HHS Public Access

Author manuscript

Environ Sci Technol. Author manuscript; available in PMC 2018 November 23.

Published in final edited form as:

Environ Sci Technol. 2017 December 19; 51(24): 14406–14416. doi:10.1021/acs.est.7b04446.

Enantioselectivity of 2,2',3,5',6-Pentachlorobiphenyl (PCB 95) Atropisomers toward Ryanodine Receptors (RyRs) and Their Influences on Hippocampal Neuronal Networks

Wei Feng^{#†}, Jing Zheng^{#†,‡}, Gaëlle Robin[†], Yao Dong[†], Makoto Ichikawa[§], Yoshihisa Inoue[§], Tadashi Mori[§], Takeshi Nakano^{||}, and Isaac N. Pessah^{*†}

[†] Molecular Biosciences, School of Veterinary Medicine, University of California, Davis, California United States

[‡] Jiangsu Provincial Key Laboratory for TCM Evaluation and Translational Development, China Pharmaceutical University, Nanjing, China

[§] Graduate School of Engineering, Osaka University, Osaka, Japan

^{||} Research Center for Environmental Preservation, Osaka University, Osaka, Japan

[#] These authors contributed equally to this work.

Abstract

Nineteen ortho-substituted PCBs are chiral and found enantioselectively enriched in ecosystems. Their differential actions on biological targets are not understood. PCB 95 (2,2',3,5',6-pentachlorobiphenyl), a chiral PCB of current environmental relevance, is among the most potent toward modifying ryanodine receptors (RyR) function and Ca²⁺ signaling. PCB 95 enantiomers are separated and assigned *aR*- and *aS*-PCB 95 using three chiral-column HPLC and circular dichroism spectroscopy. Studies of RyR1-enriched microsomes show *aR*-PCB 95 with >4× greater potency (EC₅₀ = 0.20 ± 0.05 μM), ~ 1.3× higher efficacy (B_{max} = 3.74 ± 0.07 μM) in [³H]Ryanodine-binding and >3× greater rates (R = 7.72 ± 0.31 nmol/sec/mg) of Ca²⁺ efflux compared with *aS*-PCB 95, whereas racemate has intermediate activity. *aR*-PCB 95 has modest selectivity for RyR2, and lower potency than racemate toward the RyR isoform mixture in brain membranes. Chronic exposure of hippocampal neuronal networks to nanomolar PCB 95 during a critical developmental period shows divergent influences on synchronous Ca²⁺ oscillation (SCO): *rac*-PCB 95 increasing and *aR*-PCB 95 decreasing SCO frequency at 50 nM, although the latter's effects are nonmonotonic at higher concentration. *aS*-PCB95 shows the greatest influence on inhibiting responses to 20 Hz electrical pulse trains. Considering persistence of PCB 95 in the environment, stereoselectivity toward RyRs and developing neuronal networks may clarify health risks associated with enantioisomeric enrichment of PCBs.

*Corresponding Author Phone: +1-(530)-752-6696; inpessah@ucdavis.edu.

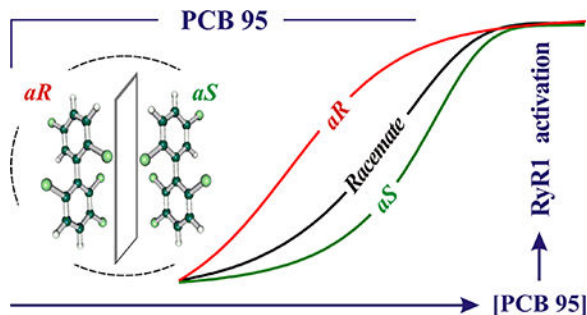
The authors declare no competing financial interest.

ASSOCIATED CONTENT

Supporting Information

The Supporting Information is available free of charge on the ACS Publications website at DOI: 10.1021/acs.est.7b04446.

Graphical Abstract



INTRODUCTION

PCBs are a group of 209 man-made chlorinated hydrocarbons. Because of their chemical, thermal stability, nonflammability, and electrical insulating properties, they were broadly included in numerous industrial and commercial applications (<https://www.epa.gov/pcbs>). Although production and use of PCBs have been banned since late 1970s, exposures continue through proximity to durable end products such as chalks in schools, dredging of PCB contaminated sediments, and inadvertent leaks from storage sites.¹ The chemical stability and bioaccumulation of PCBs in food animals and humans has been unquestionably documented.^{2–4} Several epidemiological studies of human populations have linked exposures to PCBs and chemically related persistent organic pollutants (POPs) to increased risk of certain cancers, prompting the International Agency of Research on Cancer (IARC) to classify PCBs as Group 1 carcinogens.⁵ Importantly, pre- and/or postnatal PCB exposures have been linked to a number of cognitive, behavioral, psychomotor, and metabolic deficits in humans and animal models.^{6–13} Mechanistic links between cancer promotion and neurological disorders has not been established.

Nineteen of the 209 PCB that possess three chlorine substituents confer chiral asymmetry about the biphenyl bond axis, and thus they exist as stable atropisomer or enantiomers.¹⁴ It is the ortho-substituted noncoplanar PCBs, including many of the chiral PCB congeners that originated out of the manufacturing process as racemic mixtures that continue to predominate.¹⁵ Although physicochemical processes do not promote enantiomeric enrichment of racemic PCBs,^{16–18} enrichment has been demonstrated in living organisms through mechanisms of differential absorption, distribution, biotransformation and excretion.¹⁹ More contemporary analytical results showed ample evidence of enantioselective dispositions of PCBs and related POPs not only in sediments and soils, but also in tissues of wildlife, laboratory animal, and humans.^{20–23} However, much less information is available about the consequences of enantioselective enrichments, their differential interactions with the biological targets whose physiological role, when modified, are known to induce and promote neurotoxicity. A major factor limiting our understanding of the molecular mechanisms underlying stereoselective influences of PCB enantiomers is the analytical challenges in enantiomeric separation and assignment of absolute conformation.^{24–29}

PCB 95, one of 19 chiral PCB congeners, is not only one of the more prevalent legacy congeners found in aging schools,^{30–32} but there is also evidence of contemporary sources from the pigment industry^{33–35} *Rac*-PCB 95 is also among the most potent and efficacious PCB congeners that target and modify ryanodine receptor (RyRs), microsomal Ca²⁺ channels that regulate the spatial and temporal fidelity of Ca²⁺ dynamics in a broad number of cell types, including striated muscle and neurons.^{36–40} Interactions of PCBs with RyRs exhibited stringent structural-activity relationships^{39–41} that can adversely influence aspects of neuronal connectivity,^{36,37,42,43} activities that appear to be highly stereoselective as demonstrated with PCB 136 enantiomers.^{25,26} Using postmortem brain samples and a neuronal cell culture model carrying a 15q11.2-q13.3 maternal duplication, exposures to PCB 95 have been recently shown to cause cumulative changes in epigenetic DNA hypomethylation enriched over autism candidate genes, through a mechanism that involves bivalent modification of histone H2A.Z.^{44,45} Whether such effects of PCB 95 are stereoselective at the levels of RyR engagement or cellular functions have not been demonstrated.

The present study specifically addresses the separation of PCB 95 enantiomers and demonstrates their enantioselective actions toward RyR isoforms and their differential influences on neuronal network activity in vitro.

MATERIALS AND METHODS

Chemicals.

PCB 95 (racemic) was purchased neat from AccuStandard (Lot: 010610KS; 99–100%), and *aR*-PCB 95 and *aS*-PCB 95 were separated from this racemic stock. [9,21-³H] Ryanodine specific activity 50–100 Ci/mmol was purchased from PerkinElmer (Bellerica, MA).

Separation of Enantiomers PCB 95.

A detailed description of the separation of PCB 95 enantiomers is presented in Results and Discussion.

Preparation of RyR1-Enriched Junctional Sarcoplasmic Reticulum (JSR).

All procedures with animals were approved by the UC Davis IACUC Committee. JSR membrane fraction enriched in RyR1 and SR/ER Ca²⁺ ATPase (SERCA) was isolated from fast-twitch skeletal muscles of <1 year-old male (~3 kg) New Zealand White rabbits, as previously described.^{46,47} Functional experiments reported in this study were performed on two JSR preparations isolated on different days.

Preparation of Mouse Skeletal Muscle, Cardiac Muscle and Brain Cortex Homogenates.

C57-BL/6 mice of 3–6 months were used for skeletal muscle (a pure source of RyR1), heart ventricles (a pure source of RyR2), and brain cortex (a mixture predominating in RyR1 and RyR2, with minor levels of RyR3) as described in details in Supporting Information (SI) and previously described.^{48–50} Protein concentration was determined using the DC protein assay kit (Bio-Rad, Richmond, CA).

Measurements of [³H]Ryanodine ([³H]Ry) Binding.

Equilibrium binding of [³H]Ry to the skeletal muscle (0.05 mg/mL for JSR, 0.25 mg/mL for homogenate), cardiac muscle (0.25 mg/mL) and brain cortex homogenates (0.4 mg/mL) was measured at 37 °C for 3 h as described in details in SI. Each radioligand–receptor binding experiment was performed on at least two independent membrane preparations, each in quadruplet or triplicate.

Measurements of Ca²⁺ Efflux and Ca²⁺-Induced Ca²⁺ Release (CICR).

The active uptake and passive release of Ca²⁺ from JSR membrane vesicles was measured in real-time using the Ca²⁺ sensitive metallochromic dye Arsenazo III as described in details in SI and in previous publication using dye Antipyrylazo III.⁵¹

Western Blot Analysis of Expressed RyRs in Brain Cortical Preps.

Mouse brain cortical preparations (two preps), together with positive controls of rabbit skeletal muscle JSR (one prep) and cardiac microsomal prep were used in the analysis with primary antibodies: monoclonal RyR1(34C) (1/ 200; DSHB, Reno, NA), monoclonal RyR2 (C3–33) (1/200; Abcam), polyclonal anti-RyR3 (1/100; EMD Millipore). The detailed descriptions are made in the SI.

Hippocampal Neuronal Cell Culture and Calcium Imaging.

Hippocampal cultures were obtained from postnatal day 0–1 (P0–P1) C57/BL6 male pups as described in detail in SI and in previous publication.⁵² Neuronal networks were exposed to PCBs chronically between 2 and 14 days in vitro (DIV), or acutely at 14 DIV while functional measurements were obtained.

Data Analysis.

Radioligand receptor binding data were fitted by nonlinear curve fitting using Origin software (Northampton, MA) or Graph Pad Prism software (Version 7.03; GraphPad Software Inc., San Diego, CA). Potency values were determined by nonlinear regression with three-parameter equation. For [³H]Ry analyses compared at certain concentrations and Ca²⁺ flux measurements, One-way ANOVA followed by post hoc Dunnett's test was used to analyze the data at 95% confidence intervals. For CICR measurements from RyR1-enriched JSR membrane fractions, statistical comparisons were made using unpaired *t* test.

RESULTS AND DISCUSSION

Separation of PCB 95 Enantiomers.

Given the environmental relevance of PCB 95 reviewed above and evidence indicating enantiomeric enrichment and metabolism of PCB 95, including human serum, liver, kidney, milk, feces, and guillemot eggs,^{53–59} we set out to cleanly separate the two enantiomeric forms from the racemic mixture.

The efficient separation of PCB 95 enantiomers was failed by simply applying commercially available chiral column in HPLC. However, it was successfully achieved when three chiral

columns composed of cellulose tris(4-methylbenzoate)(Daicel Corp, Japan; YMC America, Inc.) were connected in series for chiral HPLC (total length of 650 mm, Figure 1A). The assignments of (*aR*) and (*aS*) enantiomers were achieved by comparing their experimental circular dichroisms with the corresponding theoretical counterparts at the RI-CC2/aug-TZVPP//DFT-D3(BJ)-TPSS/def-TZVP level, as described previously.⁶⁰ Accordingly, the first elute was assigned as the *aR* enantiomer (Figure 1C, left). It is interesting note that the pattern of Cotton effects observed in their CD spectra for PCB 95 was mostly reversed in sign when compared with that of PCB183 (Figure 1C, right),⁶⁰ given the same absolute configurations. It is ascribable to the reversal of transition dipole moments in the latter species with respect to the chlorine atoms at para positions.

Using different chiral columns packed with polysaccharides derivatives, Xu. et al. separated PCB 95 enantiomers, with purities >98% (Publication in Chinese; Abstract in English).⁶¹ Utilizing online optical rotation detector (IBZMESSTECHNIK, Germany), they assigned the absolute configurations for enantiomers of first elute as (–)-PCB 95 and the second (+)-PCB95.⁶¹ We therefore propose *aR* is equivalent to (–)-PCB 95 and *aS*-PCB 95 is equivalent to (+)-PCB 95.

Enantiomeric enrichments is expressed as EF (enantiomeric fraction), the concentration of one enantiomer divided by the total concentration of both enantiomers ($EF = A1/(A1+A2)$, with 0.5 corresponding to racemic mixture).⁶² Enantiomeric enrichment of PCB 95 was found with an EF value as high as 0.693 ± 0.172 in the serum samples of E-waste recycling workers in China;⁵⁸ 0.64–0.76 in the samples from human milk in Switzerland;⁵⁶ 0.51–0.75 from liver, 0.50–0.57 from kidney in Belgium.⁵⁴

PCB 95 Enantiomers Differentially Sensitize [³H]Ry Binding to RyRs.

[³H]Ryanodine ([³H]Ry) binds with nanomolar affinity to RyRs that are anchored within the endoplasmic/sarcoplasmic reticulum (ER/SR) of neurons and muscle, respectively.^{46,63–65} Since [³H]Ry interactions with RyRs have been shown to be highly specific, and exhibit binding kinetics that were highly sensitive to the conformational states of the Ca²⁺ channel complex, [³H]Ry binding has been broadly used to identify and quantify the influences of ligands that allosterically modulate channel function, positively and/or negatively. It has been used to develop a quantitative structure–activity relationship among PCB congeners with RyR preparations from mammals and fish,^{38,40,41} although the stereoselectivity of chiral PCBs of environmental relevance has remained poorly understood. In previous studies, racemic PCB 95 was shown to significantly increases maximal [³H]Ry binding capacity (B_{max}) and affinity⁵¹ by stabilizing the high affinity state of RyR1, an effect demonstrated with the purified channel protein.⁶⁶ To determine whether and to what degree PCB 95 stereoisomers influence the conformation of RyR1, we used concentrations of [³H]Ry that itself does not influence receptor conformation (i.e., 10 nM)^{67,68} and performed equilibrium [³H]Ry binding analysis to compare enantioselectivity by *rac*-, *aR*-, or *aS*-PCB 95 toward tissues that express RyR1 (skeletal muscle), RyR2 (cardiac muscle), or a mixture of all three RyR isoforms (brain cortex).

Figure 2 showed that the [³H]Ry bound to RyR1 was highly dependent on the PCB 95 concentration when RyR1-enriched JSR is used as target. Most significantly, *aR*- was

nearly 5-fold more potent and 30% more efficacious than *aS*-PCB 95 in enhancing the specific [³H]Ry binding, whereas *rac*-PCB 95 had intermediate activity (Figure 2A and B). Even at a low concentration of 0.2 μ M, *aR* resulted in 3- and >2-fold greater receptor occupancy compared to *aS*- and *rac*-PCB 95, respectively (Figure 2A insert). These data showed a clear stereoselectivity for interaction of PCB 95 enantiomers toward RyR1.

To test our hypothesis whether the stereoselectivity observed toward RyR1 extended to preparations that express only RyR2 or complex mixtures of RyRs present in brain tissue, membrane homogenates from 110,000xg pellets were assayed as described in SI and Materials and Methods. For consistency, western blot and [³H]Ry binding analyses were performed to compare homogenates prepared from mouse skeletal muscle, heart and brain cortex in parallel. Cortical preparations were probed with selective antibodies at saturating levels by western blot analysis and skeletal and cardiac membranes served as positive controls for RyR1 and RyR2. All three isoforms (RyR1, RyR2, and RyR3) were detected in brain cortical preparations (SI Figure 1), and qualitatively the levels followed the rank order in abundance RyR2 > RyR1 > RyR3. The relative abundance of RyR isoforms expressed cerebellum, cortex and hippocampus has not been clearly established.⁶⁹ Although RyR1 has not been consistently shown to be expressed in cortex,^{70–72} our results clearly affirm its presence (SI Figure 1). The [³H]Ry binding density of these preparations were approximately 16.4–54-fold lower than those measured with JSR preparations. The high lipid-to-protein content in these less-pure preparations decreased the apparent potencies for PCBs in binding assays, presumably due to lipid partitioning⁴⁰ and it was therefore difficult to titrate free PCB 95 to concentrations sufficient to saturate its activating effects on RyR1. Nevertheless, the results obtained from these mouse RyR1 preparations were consistent with those obtained with rabbit JSR, with *aR*-PCB 95 exhibiting higher potency and efficacy than either *rac*- or *aS*-PCB 95 (Figure 3A). Although RyR2 preparations showed much narrower selectivity among the three PCB 95 forms, *aR*-PCB 95 exhibited 15.4% (**p* = 0.05 vs *rac*-PCB95) higher activity toward RyR2 at 1.5 μ M compared to racemate, while no significance was found between the activity of *aS* and racemate toward RyR2, and *aR*-PCB 95 possessing higher potency than *rac*- and *aS*-PCB 95 (Figure 3B), consistent with the observations from in RyR1 binding analyses. Unexpectedly, the combination of all three RyR isoforms known to be expressed in the brain, resulted in a distinct pattern of activity with rank order of *rac* > *aS*-PCB 95 > *aR*-PCB 95, with *aR*-PCB 95 and *aS*-PCB 95 at 0.2 μ M exhibiting 43.1% (***) and 22.4% (**p* = 0.05 vs *rac*-PCB95) lower activity toward brain RyRs compared with racemate, respectively (Figure 3B).

PCB 95 Enantiomers Differentially Alter Microsomal Ca²⁺ Transport.

Consistent with their direct RyR-activating properties, noncoplanar PCBs have been shown to selectively trigger net Ca²⁺ release from JSR^{49,73} and from brain microsomes⁴⁹ without inhibiting SERCA activity, in a manner prevented with RyR blockers. In this study, we interrogated the possible stereoselectivity of *aR*- and *aS*- compared to *rac*-PCB 95 on Ca²⁺ fluxes using the metallochromic Ca²⁺ dye Arsenazo III and in the presence of active SERCA pump-dependent vesicular Ca²⁺ uptake as depicted in the Figure 4A. After 180 nmole Ca²⁺ were sequentially loaded into the JSR (Figure 4B), addition of DMSO (vehicle, 0.5%) did not elicit a release of actively accumulated Ca²⁺ (Figure 4B, gray trace). However, addition

of *aR*-PCB 95 (5 μ M) triggered a nearly 3-fold higher rate of Ca^{2+} efflux compared to *aS*-PCB 95, whereas the rate elicited by *rac*-PCB 95 was intermediate (Figure 4B and C). Compared to racemate, the initial rate of Ca^{2+} release elicited by *aR*-PCB 95 and *aS*-PCB 95 are 70.9% (***) $p < 0.001$ vs *rac*-PCB95) faster and 38.6% (***) $p < 0.001$ vs *rac*-PCB95) slower, respectively (Figure 4D).

RyR isoforms in combination with inositol 1,4,5-trisphosphate receptor (IP_3R) have been shown to mediate a physiological process CICR, representing a fundamentally important Ca^{2+} signaling mechanism in a broad numbers of cell types.^{38,74–77} Previous study has shown that racemic PCB 95 enhances CICR by increasing the sensitivity of RyR1 to Ca^{2+} .⁵¹ We therefore used JSR to test whether PCB 95 enantioselectively influenced CICR. Figure 5 showed that JSR actively loaded with Ca^{2+} to $\sim 70\%$ of their capacity retain accumulated Ca^{2+} when either DMSO (0.5%) or a low concentration (250 nM) of PCB 95 is introduced 2.5 min prior to eliciting CICR by addition of 90 nmol Ca^{2+} to the vesicle medium (Figure 5A). Their presence enhanced CICR with the rank potency: *aR*-PCB > *rac* > *aS*-PCB 95 > DMSO (Figure 5B and C).

In general, the stereoselectivities observed with *aR*- over *aS*-PCB 95 in both [^3H]Ry binding and Ca^{2+} flux assays were in very good agreement with our previous results obtained with enantiomers of the less environmentally relevant congener PCB 136.²⁵ In this regard, *aR*-PCB 95, which we presume is (–)-PCB 95 based on the results of Xu and co-workers,⁶¹ is more active toward the major isoforms RyR1 and RyR2 when expressed individually, consistent with the stereoselectivity assigned for PCB 136 enantiomers.²⁵ However, it should be emphasized that (1) the separation in potency and efficacy of (–)- over (+)-PCB 136 toward RyR1 and RyR2 was significantly more pronounced compared to our current findings with *aR*- over *aS*-PCB 95, and (2) the greater relative potency of *rac*-PCB 95 compared to either enantiomeric form where multiple RyR isoforms are expressed, as they are in brain and several other tissues. Nevertheless, the stereoselectivity of PCB 95 enantiomers identified here was significant because PCB 95 has been shown to predominate in recent sampling of many grade schools,³² human breast milk, blood and other tissues, and some found enantioselectively enriched.^{54,58,78–80} Typically noncoplanar PCBs were found to be more persistent with half-lives in human body ranging from 0.4 to 3 years^{78,81} and metabolic elimination rates averaging about 6 years.⁸²

PCB 95 Enantiomers Differentially Alter Ca^{2+} Dynamics in Hippocampal Neurons.

How the observed pattern of stereoselectivity toward RyRs for PCB 95 translated to their ability to alter Ca^{2+} signals is known to be important for regulating excitability, but the proper development of neuronal networks⁸³ has not been previously investigated. Single cell real-time Ca^{2+} imaging techniques were therefore used to measure both acute responses in terms of neuronal network excitability, as well as the consequences of chronic exposure (12 days in vitro; from 2 to 14 DIV). Two functional end points were measured in neuronal cultures from mouse hippocampus, (1) patterns of SOCs known to be important for long-term activity-dependent neuronal plasticity, and (2) properties of Ca^{2+} transients evoked by electrical stimulation. For acute responses, SCO patterns were analyzed from mature networks at 14 DIV 10 min before and after focal perfusion of vehicle or PCB 95 (500 nM)

(Figure 6A). At 14 DIV, neurons maintained well-defined SCO activity and addition of DMSO did not significantly alter SCO frequency (Figure 6B) or Ca^{2+} transient amplitudes by electrical pulses at 20 Hz (Figure 6D), although DMSO did reduce SCO amplitude by ~15% (Figure 6C; $p < 0.01$). Acute application of *rac*-PCB 95 significantly increased SCO frequency 14% higher than control (DMSO; $p < 0.01$), but neither *aS*- nor *aR*-PCB 95 had significant influence (Figure 6B). In contrast, all three PCB 95 preparations reduced SCO amplitudes compared to DMSO-control with the rank order of *aS*- > *aR*- > *rac* (Figure 6C; reductions of 8.5, 21, and 39%, respectively), whereas only *aS*-PCB 95 caused a 35% ($p < 0.01$) reduction in Ca^{2+} transient amplitudes triggered at 20 Hz electrical (Figure 6D).

The hippocampal neuronal culture model was also used to test the differential influences of prolonged (2–14 DIV) exposure to lower PCB 95 (50 or 200 nM). Under these conditions, chronic exposure to DMSO alone according to the chronic treatment protocol did not alter any aspect of SCO dynamics measured in this study (Figure 7A–G). Interestingly, chronic exposure to either 50 or 200 nM *rac*-PCB 95 elicited the largest increases in SCO frequency (2.1- and 1.9-fold of control, respectively) (Figure 7B,E), without significantly altering either SCO amplitudes or Ca^{2+} transient amplitudes evoked by 20 Hz electrical pulse trains (Figure 7C,F vs D,G). In contrast, neurons responded to chronic *aR*-PCB 95 exposure in a nonmonotonic manner with 50 nM inhibiting SCO frequency by 64% and 200 nM having no significant effect (Figure 7B,E), although exposure to both concentrations increased SCO amplitudes comparably (25%) (Figure 7C,F). *aR*-PCB 95 only at the higher concentration (200 nM) modestly increased by ~15% compared to DMSO vehicle the amplitude of Ca^{2+} transients evoked with 20 Hz electrical pulses (Figure 7D,G). By comparison, only chronic exposure to 200 nM *aS*-PCB 95 increased SCO frequency 1.8-fold over vehicle control (Figure 7B,E). Both low and high concentrations of *aS*-PCB 95 reduced SCO amplitudes (25 and 38% reductions compared to vehicle, respectively) (Figure 7C,F), and reduced the amplitudes of electrically evoked Ca^{2+} transients by 39 and 23%, respectively (Figure 7D,G).

Taken together, these data clearly demonstrated for the first time that (1) *aR*- was more potent than *aS*-PCB 95 toward stabilizing the open state of RyR1 and RyR2, although the stereoselectivity was much greater with RyR1 in both [^3H]Ry and microsomal Ca^{2+} flux assays, and (2) a complex mixture of all three isoforms found in brain tissues produced a unique signature with the racemic mixture having the greatest potency and only modest selectivity toward *aS*- over *aR*-PCB 95. Consistent with the structure–activity relationship toward RyRs in brain tissue, the SCO patterns measured in developed neuronal networks were highly sensitive to acute exposure to *rac*-PCB 95, which both increased their frequency and decreased their amplitude, whereas each enantiomers only reduced SCO amplitude with similar magnitude. Electrically evoked Ca^{2+} transients used to test the integrity of excitatory neurotransmission revealed that only *aS*-PCB 95 reduced the Ca^{2+} transients amplitude with the acute exposure protocol used in our study. These results not only demonstrated differential enantioselectivity toward RyR1 and RyR2, the major isoforms expressed in the brain, but more importantly, underscored the complex spatial patterns of expression of all three RyR isoforms within neural networks (presynaptic, postsynaptic, somal), which are defined presumably by the functional contribution of each isoform toward sculpting SCO and evoked Ca^{2+} transients properties.^{13,38,84}

Perhaps a more relevant model of real-world exposures in humans and animals, were the results from chronic exposure between 2 and 14 DIV. During this in vitro time frame, neurons recapitulated morphologic, neurochemical, and functional attributes known to occur in the developing hippocampus.^{13,85}

Under these more realistic exposure conditions, nanomolar *aS*-PCB 95 proved to be most potent toward altering electrically evoked Ca²⁺ transient amplitude. However, all three forms of PCB 95 tested differentially altered spontaneous synchronous Ca²⁺ oscillations (SCO dynamics) depending on concentration, which is likely the result of their divergent influences the three RyR isoforms expressed in the brain that differentially impacted neuronal network maturity and connectivity during the 12-day exposure. This interpretation is plausible given that both RyR1 and RyR2 have been shown to influence activity dependent plasticity and synaptogenesis by exposure to *rac*-PCB 95 and many of these effects showed a nonmonotonic concentrationeffect relationship that could be driven by the enantiomeric selectivity described here.^{36,37,86,87} These effects of *rac*-PCB 95 could be eliminated by siRNA mediated knockdown of either RyR1 or RyR2,³⁶ indicating that normal expression of RyR1 and RyR2 were necessary to fully manifest PCB 95-mediated alterations of neuronal growth patterns, which are known to be highly Ca²⁺ dependent process. Furthermore, exposing rat dams during pregnancy to *rac*-PCB 95 persistently impaired not only spatial learning, memory⁸⁸ and hippocampal excitability,⁸⁹ but also altered proper development of neural network circuitry of the primary auditory cortex, resulting in abnormal tonotopy, receptive fields and long-lived excitatory-inhibitory imbalance⁴² in the exposed offspring. Finally, Yang and co-workers⁴³ using a developmental PCB exposure model in rats, which identified links among abnormal patterns of spatial learning, dendritic growth, plasticity, RyR expression and function. Again these finding indicated a nonmonotonic dose–response relationship. Base on the findings reported here, it is plausible that the complex developmental outcomes reported in previous in vitro and in vivo studies could, at least in part, be driven by stereoselective modification of multiple RyR isoforms expressed in the developing brain.

Supplementary Material

Refer to Web version on PubMed Central for supplementary material.

ACKNOWLEDGMENTS

Supported by the National institute of Environmental Health Sciences (R01 ES014901, P01 ES011269, and P42 ES04699), and China Scholarship Council (CSC 201507060027). We thank Dr. Birgit Puschner of the UC Davis Bioanalytic Research Core for verification of the purity of commercially purchased PCB 95 racemate (99%).

REFERENCES

- (1). Chatel G; Naffrechoux E; Draye M Avoid the PCB mistakes: A more sustainable future for ionic liquids. *J. Hazard. Mater.* 2017, 324 (Pt B), 773–780. [PubMed: 28992570]
- (2). Annamalai J; Namasivayam V Endocrine disrupting chemicals in the atmosphere: Their effects on humans and wildlife. *Environ. Int.* 2015, 76, 78–97. [PubMed: 25569353]
- (3). Arnot JA; Quinn CL Development and evaluation of a database of dietary bioaccumulation test data for organic chemicals in fish. *Environ. Sci. Technol.* 2015, 49 (8), 4783–96. [PubMed: 25821900]

- 4). Manzetti S; van der Spoel ER; van der Spoel D Chemical properties, environmental fate, and degradation of seven classes of pollutants. *Chem. Res. Toxicol.* 2014, 27 (5), 713–37. [PubMed: 24646038]
- 5). Lauby-Secretan B; Loomis D; Baan R; El Ghissassi F; Bouvard V; Benbrahim-Tallaa L; Guha N; Grosse Y; Straif K Use of mechanistic data in the IARC evaluations of the carcinogenicity of polychlorinated biphenyls and related compounds. *Environ. Sci. Pollut. Res.* 2016, 23 (3), 2220–9.
- 6). Berghuis SA; Bos AF; Sauer PJ; Roze E Developmental neurotoxicity of persistent organic pollutants: an update on childhood outcome. *Arch. Toxicol.* 2015, 89 (5), 687–709. [PubMed: 25618547]
- 7). Ghosh S; Murinova L; Trnovec T; Loffredo CA; Washington K; Mitra PS; Dutta SK Biomarkers linking PCB exposure and obesity. *Curr. Pharm. Biotechnol.* 2014, 15 (11), 1058–68. [PubMed: 25420728]
- 8). Bell MR Endocrine-disrupting actions of PCBs on brain development and social and reproductive behaviors. *Curr. Opin. Pharmacol.* 2014, 19, 134–44. [PubMed: 25310366]
- 9). Grandjean P; Landrigan PJ Neurobehavioural effects of developmental toxicity. *Lancet Neurol.* 2014, 13 (3), 330–8. [PubMed: 24556010]
- 10). El Majidi N; Bouchard M; Carrier G Systematic analysis of the relationship between standardized biological levels of polychlorinated biphenyls and thyroid function in pregnant women and newborns. *Chemosphere* 2014, 98, 1–17. [PubMed: 24200047]
- 11). van Thriel C; Westerink RH; Beste C; Bale AS; Lein PJ; Leist M Translating neurobehavioural endpoints of developmental neurotoxicity tests into in vitro assays and readouts. *Neurotoxicology* 2012, 33 (4), 911–24. [PubMed: 22008243]
- 12). Bal-Price A; Crofton KM; Sachana M; Shafer TJ; Behl M; Forsby A; Hargreaves A; Landesmann B; Lein PJ; Louise J; Monnet-Tschudi F; Paini A; Rolaki A; Schrattenholz A; Sunol C; van Thriel C; Whelan M; Fritsche E Putative adverse outcome pathways relevant to neurotoxicity. *Crit. Rev. Toxicol.* 2015, 45 (1), 83–91. [PubMed: 25605028]
- 13). Stamou M; Streifel KM; Goines PE; Lein PJ Neuronal connectivity as a convergent target of gene x environment interactions that confer risk for Autism Spectrum Disorders. *Neurotoxicol. Teratol.* 2013, 36, 3–16. [PubMed: 23269408]
- 14). Kaiser K On the optical activity of polychlorinated biphenyls. *Environ. Pollut.* 1974, 7 (2), 93–101.
- 15). Robson M; Harrad S Chiral PCB signatures in air and soil: implications for atmospheric source apportionment. *Environ. Sci. Technol.* 2004, 38 (6), 1662–6. [PubMed: 15074672]
- 16). Asher BJ; Ross MS; Wong CS Tracking chiral polychlorinated biphenyl sources near a hazardous waste incinerator: fresh emissions or weathered revolatilization? *Environ. Toxicol. Chem.* 2012, 31 (7), 1453–60. [PubMed: 22544627]
- 17). Asher BJ; Wong CS; Rodenburg LA Chiral source apportionment of polychlorinated biphenyls to the Hudson River estuary atmosphere and food web. *Environ. Sci. Technol.* 2007, 41 (17), 6163–9. [PubMed: 17937297]
- 18). Jamshidi A; Hunter S; Hazrati S; Harrad S Concentrations and chiral signatures of polychlorinated biphenyls in outdoor and indoor air and soil in a major U.K. conurbation. *Environ. Sci. Technol.* 2007, 41 (7), 2153–8. [PubMed: 17438756]
- 19). Müller TA; Kohler HP Chirality of pollutants—effects on metabolism and fate. *Appl. Microbiol. Biotechnol.* 2004, 64 (3), 300–316. [PubMed: 14716466]
- 20). Zhang Y; Ye J; Liu M Enantioselective Biotransformation of Chiral Persistent Organic Pollutants. *Curr. Protein Pept. Sci.* 2017, 18 (1), 48–56. [PubMed: 27072397]
- 21). Zheng XB; Luo XJ; Zeng YH; Wu JP; Mai BX Chiral polychlorinated biphenyls (PCBs) in bioaccumulation, maternal transfer, and embryo development of chicken. *Environ. Sci. Technol.* 2015, 49 (2), 785–91. [PubMed: 25525742]
- 22). Wu X; Barnhart C; Lein PJ; Lehmler HJ Hepatic metabolism affects the atropselective disposition of 2,2',3,3',6,6' hexachlorobiphenyl (PCB 136) in mice. *Environ. Sci. Technol.* 2015, 49 (1), 616–25. [PubMed: 25420130]

- 23). Kania-Korwel I; Lukasiewicz T; Barnhart CD; Stamou M; Chung H; Kelly KM; Bandiera S; Lein PJ; Lehmler HJ Congener-Specific Disposition of Chiral Polychlorinated Biphenyls in Lactating Mice and Their Offspring: Implications for PCB Developmental Neurotoxicity. *Toxicol. Sci.* 2017, 158, 101. [PubMed: 28431184]
- 24). Lehmler HJ; Robertson LW; Garrison AW; Kodavanti PR Effects of PCB 84 enantiomers on [3H]-phorbol ester binding in rat cerebellar granule cells and 45Ca²⁺-uptake in rat cerebellum. *Toxicol. Lett.* 2005, 156 (3), 391–400. [PubMed: 15763638]
- 25). Pessah IN; Lehmler HJ; Robertson LW; Perez CF; Cabrales E; Bose DD; Feng W Enantiomeric specificity of (–)-2,2',3,3',6,6'-hexachlorobiphenyl toward ryanodine receptor types 1 and 2. *Chem. Res. Toxicol.* 2009, 22 (1), 201–7. [PubMed: 18954145]
- 26). Yang D; Kania-Korwel I; Ghogha A; Chen H; Stamou M; Bose DD; Pessah IN; Lehmler HJ; Lein PJ PCB 136 atropselectively alters morphometric and functional parameters of neuronal connectivity in cultured rat hippocampal neurons via ryanodine receptor-dependent mechanisms. *Toxicol. Sci.* 2014, 138 (2), 379–92. [PubMed: 24385416]
- 27). Xu N; Mu P; Yin Z; Jia Q; Yang S; Qian Y; Qiu J Analysis of the Enantioselective Effects of PCB95 in Zebrafish (*Danio rerio*) Embryos through Targeted Metabolomics by UPLC-MS/MS. *PLoS One* 2016, 11 (8), e0160584. [PubMed: 27500732]
- 28). Kania-Korwel I; Barnhart CD; Lein PJ; Lehmler HJ Effect of pregnancy on the disposition of 2,2',3,5',6-pentachlorobiphenyl (PCB 95) atropisomers and their hydroxylated metabolites in female mice. *Chem. Res. Toxicol.* 2015, 28 (9), 1774–83. [PubMed: 26271003]
- 29). Kania-Korwel I; Lehmler HJ Toxicokinetics of chiral polychlorinated biphenyls across different species—a review. *Environ. Sci. Pollut. Res.* 2016, 23 (3), 2058–80.
- 30). Herrick RF; Stewart JH; Allen JG Review of PCBs in US schools: a brief history, an estimate of the number of impacted schools, and an approach for evaluating indoor air samples. *Environ. Sci. Pollut. Res.* 2016, 23 (3), 1975–85.
- 31). Osterberg D; Scammell MK PCBs in schools—where communities and science come together. *Environ. Sci. Pollut. Res.* 2016, 23 (3), 1998–2002.
- 32). Thomas KXJ; Williams R; P Jones P; Whitaker D, Polychlorinated Biphenyls (PCBs) in School Buildings: Sources, Environmental Levels, and Exposures. EPA/600/R-12/051/ September 30, 2012.
- 33). Koh WX; Hornbuckle KC; Thorne PS Human Serum from Urban and Rural Adolescents and Their Mothers Shows Exposure to Polychlorinated Biphenyls Not Found in Commercial Mixtures. *Environ. Sci. Technol.* 2015, 49 (13), 8105–12. [PubMed: 26053216]
- 34). Anezaki K; Kannan N; Nakano T Polychlorinated biphenyl contamination of paints containing polycyclic- and Naphthol AS-type pigments. *Environ. Sci. Pollut. Res.* 2015, 22 (19), 14478–88.
- 35). Hu D; Hornbuckle KC Inadvertent polychlorinated biphenyls in commercial paint pigments. *Environ. Sci. Technol.* 2010, 44 (8), 2822–7. [PubMed: 19957996]
- 36). Wayman GA; Yang D; Bose DD; Lesiak A; Ledoux V; Bruun D; Pessah IN; Lein PJ PCB-95 promotes dendritic growth via ryanodine receptor-dependent mechanisms. *Environ. Health Perspect.* 2012, 120 (7), 997–1002. [PubMed: 22534141]
- 37). Wayman GA; Bose DD; Yang D; Lesiak A; Bruun D; Impey S; Ledoux V; Pessah IN; Lein PJ PCB-95 modulates the calcium-dependent signaling pathway responsible for activity-dependent dendritic growth. *Environ. Health Perspect.* 2012, 120 (7), 1003–9. [PubMed: 22534176]
- 38). Chen Y; Tassone F; Berman RF; Hagerman PJ; Hagerman RJ; Willemsen R; Pessah IN Murine hippocampal neurons expressing Fmr1 gene premutations show early developmental deficits and late degeneration. *Hum. Mol. Genet.* 2010, 19 (1), 196–208. [PubMed: 19846466]
- 39). Niknam Y; Feng W; Cherednichenko G; Dong Y; Joshi SN; Vyas SM; Lehmler HJ; Pessah IN Structure-activity relationship of selected meta- and para-hydroxylated non-dioxin like polychlorinated biphenyls: from single RyR1 channels to muscle dysfunction. *Toxicol. Sci.* 2013, 136 (2), 500–13. [PubMed: 24014653]
- 40). Holland EB; Feng W; Zheng J; Dong Y; Li X; Lehmler HJ; Pessah IN An Extended Structure-Activity Relationship of Nondioxin-Like PCBs Evaluates and Supports Modeling Predictions and Identifies Picomolar Potency of PCB 202 Towards Ryanodine Receptors. *Toxicol. Sci.* 2017, 155 (1), 170–181. [PubMed: 27655348]

- 41). Pessah IN; Hansen LG; Albertson TE; Garner CE; Ta TA; Do Z; Kim KH; Wong PW Structure-activity relationship for noncoplanar polychlorinated biphenyl congeners toward the ryanodine receptor-Ca²⁺ channel complex type 1 (RyR1). *Chem. Res. Toxicol.* 2006, 19 (1), 92–101. [PubMed: 16411661]
- 42). Kenet T; Froemke RC; Schreiner CE; Pessah IN; Merzenich MM Perinatal exposure to a noncoplanar polychlorinated biphenyl alters tonotopy, receptive fields, and plasticity in rat primary auditory cortex. *Proc. Natl. Acad. Sci. U. S. A.* 2007, 104 (18), 7646–51. [PubMed: 17460041]
- 43). Yang D; Kim KH; Phimister A; Bachstetter AD; Ward TR; Stackman RW; Mervis RF; Wisniewski AB; Klein SL; Kodavanti PR; Anderson KA; Wayman G; Pessah IN; Lein PJ Developmental exposure to polychlorinated biphenyls interferes with experience-dependent dendritic plasticity and ryanodine receptor expression in weanling rats. *Environ. Health Perspect.* 2009, 117 (3), 426–35. [PubMed: 19337518]
- 44). Mitchell MM; Woods R; Chi LH; Schmidt RJ; Pessah IN; Kostyniak PJ; LaSalle JM Levels of select PCB and PBDE congeners in human postmortem brain reveal possible environmental involvement in 15q11-q13 duplication autism spectrum disorder. *Environmental and molecular mutagenesis* 2012, 53 (8), 589–98. [PubMed: 22930557]
- 45). Dunaway KW; Islam MS; Coulson RL; Lopez SJ; Vogel Ciernia A; Chu RG; Yasui DH; Pessah IN; Lott P; Mordaunt C; Meguro-Horike M; Horike SI; Korf I; LaSalle JM Cumulative Impact of Polychlorinated Biphenyl and Large Chromosomal Duplications on DNA Methylation, Chromatin, and Expression of Autism Candidate Genes. *Cell Rep* 2016, 17 (11), 3035–3048. [PubMed: 27974215]
- 46). Pessah IN; Anderson KW; Casida JE Solubilization and separation of Ca²⁺-ATPase from the Ca²⁺-ryanodine receptor complex. *Biochem. Biophys. Res. Commun.* 1986, 139 (1), 235–43. [PubMed: 2945551]
- 47). Saito A; Seiler S; Chu A; Fleischer S Preparation and morphology of sarcoplasmic reticulum terminal cisternae from rabbit skeletal muscle. *J. Cell Biol.* 1984, 99 (3), 875–85. [PubMed: 6147356]
- 48). Zimanyi I; Pessah IN Pharmacological characterization of the specific binding of [3H]ryanodine to rat brain microsomal membranes. *Brain Res.* 1991, 561 (2), 181–91. [PubMed: 1666327]
- 49). Wong PW; Brackney WR; Pessah IN Ortho-substituted polychlorinated biphenyls alter microsomal calcium transport by direct interaction with ryanodine receptors of mammalian brain. *J. Biol. Chem.* 1997, 272 (24), 15145–53. [PubMed: 9182535]
- 50). Berridge MJ Calcium regulation of neural rhythms, memory and Alzheimer's disease. *J. Physiol.* 2014, 592 (2), 281–93. [PubMed: 23753528]
- 51). Wong PW; Pessah IN Ortho-substituted polychlorinated biphenyls alter calcium regulation by a ryanodine receptor-mediated mechanism: structural specificity toward skeletal- and cardiac-type microsomal calcium release channels. *J. Biol. Chem.* 1996, 271 (4), 740–51.
- 52). Robin G; Lopez JR; Espinal GM; Hulsizer S; Hagerman PJ; Pessah IN Calcium dysregulation and Cdk5-ATM pathway involved in a mouse model of fragile X-associated tremor/ataxia syndrome. *Hum. Mol. Genet.* 2017, 26 (14), 2649–2666. [PubMed: 28444183]
- 53). Zheng J; Yan X; Chen SJ; Peng XW; Hu GC; Chen KH; Luo XJ; Mai BX; Yang ZY Polychlorinated biphenyls in human hair at an e-waste site in China: composition profiles and chiral signatures in comparison to dust. *Environ. Int.* 2013, 54, 128–33. [PubMed: 23454108]
- 54). Chu S; Covaci A; Schepens P Levels and chiral signatures of persistent organochlorine pollutants in human tissues from Belgium. *Environ. Res.* 2003, 93 (2), 167–76. [PubMed: 12963401]
- 55). Bordajandi LR; Gonzalez MJ Enantiomeric fraction of selected chiral polychlorinated biphenyls in cow, goat, and ewe milk and dairy products by heart-cut multidimensional gas chromatography: first results. *J. Dairy Sci.* 2008, 91 (2), 483–9. [PubMed: 18218734]
- 56). Bucheli TD; Brandli RC Two-dimensional gas chromatography coupled to triple quadrupole mass spectrometry for the unambiguous determination of atropisomeric polychlorinated biphenyls in environmental samples. *Journal of chromatography. A* 2006, 1110 (1–2), 156–64. [PubMed: 16472816]

- 57). Harrad S; Ren J; Hazrati S; Robson M Chiral signatures of PCB#s 95 and 149 in indoor air, grass, duplicate diets and human faeces. *Chemosphere* 2006, 63 (8), 1368–76. [PubMed: 16289232]
- 58). Zheng J; Yu LH; Chen SJ; Hu GC; Chen KH; Yan X; Luo XJ; Zhang S; Yu YJ; Yang ZY; Mai BX Polychlorinated Biphenyls (PCBs) in Human Hair and Serum from EWaste Recycling Workers in Southern China: Concentrations, Chiral Signatures, Correlations, and Source Identification. *Environ. Sci. Technol.* 2016, 50 (3), 1579–86. [PubMed: 26757157]
- 59). Uwimana E; Li X; Lehmler HJ 2,2',3,5',6-Pentachlorobiphenyl (PCB 95) Is Atropselectively Metabolized to para-Hydroxylated Metabolites by Human Liver Microsomes. *Chem. Res. Toxicol.* 2016, 29 (12), 2108–2110. [PubMed: 27989147]
- 60). Toda M; Matsumura C; Tsurukawa M; Okuno T; Nakano T; Inoue Y; Mori T Absolute configuration of atropisomeric polychlorinated biphenyl 183 enantiomerically enriched in human samples. *J. Phys. Chem. A* 2012, 116 (37), 9340–6. [PubMed: 22917060]
- 61). Xu NN, M, P. Q., Jia Q, Chai TT, Yin ZQ, Yang SM, Qiu J, Comparison of Enantioseparations of 19 Chiral Polychlorinated Biphenyls by 5 Different Polysaccharides Chiral Columns. *Chinese J. Anal. Chemi* 2015, 43, (6), 795–801 (In Chinese; Abstract in English; http://online.analchem.cn:8080/fxhx/EN/volumn/volumn_453.htm).
- 62). De Geus HJ; Wester PG; de Boer J; Brinkman UA Enantiomer fractions instead of enantiomer ratios. *Chemosphere* 2000, 41 (5), 725–7. [PubMed: 10834374]
- 63). Pessah IN; Waterhouse AL; Casida JE The calciumryanodine receptor complex of skeletal and cardiac muscle. *Biochem. Biophys. Res. Commun.* 1985, 128 (1), 449–56. [PubMed: 3985981]
- 64). Pessah IN; Stambuk RA; Casida JE Ca²⁺-activated ryanodine binding: mechanisms of sensitivity and intensity modulation by Mg²⁺, caffeine, and adenine nucleotides. *Molecular pharmacology* 1987, 31 (3), 232–8. [PubMed: 2436032]
- 65). Waterhouse AL; Pessah IN; Francini AO; Casida JE Structural aspects of ryanodine action and selectivity. *J. Med. Chem.* 1987, 30 (4), 710–6. [PubMed: 2435905]
- 66). Samsó M; Feng W; Pessah IN; Allen PD Coordinated movement of cytoplasmic and transmembrane domains of RyR1 upon gating. *PLoS Biol.* 2009, 7 (4), e85. [PubMed: 19402748]
- 67). Zimanyi I; Buck E; Abramson JJ; Mack MM; Pessah IN Ryanodine induces persistent inactivation of the Ca²⁺ release channel from skeletal muscle sarcoplasmic reticulum. *Molecular pharmacology* 1992, 42 (6), 1049–57. [PubMed: 1480132]
- 68). Buck E; Zimanyi I; Abramson JJ; Pessah IN Ryanodine stabilizes multiple conformational states of the skeletal muscle calcium release channel. *J. Biol. Chem.* 1992, 267 (33), 23560–7. [PubMed: 1331089]
- 69). Meissner G Regulation of mammalian ryanodine receptors. *Front. Biosci., Landmark Ed* 2002, 7, d2072–80.
- 70). Giannini G; Conti A; Mammarella S; Scrobogna M; Sorrentino V The ryanodine receptor/calcium channel genes are widely and differentially expressed in murine brain and peripheral tissues. *J. Cell Biol.* 1995, 128 (5), 893–904. [PubMed: 7876312]
- 71). Kurokawa K; Mizuno K; Kiyokage E; Shibasaki M; Toida K; Ohkuma S Dopamine D1 receptor signaling system regulates ryanodine receptor expression after intermittent exposure to methamphetamine in primary cultures of midbrain and cerebral cortical neurons. *J. Neurochem.* 2011, 118 (5), 773–83. [PubMed: 21707617]
- 72). Galeotti N; Quattrone A; Vivoli E; Norcini M; Bartolini A; Ghelardini C Different involvement of type 1, 2, and 3 ryanodine receptors in memory processes. *Learn. Mem.* 2008, 15 (5), 315–23. [PubMed: 18441289]
- 73). Wong PW; Pessah IN Noncoplanar PCB 95 alters microsomal calcium transport by an immunophilin FKBP12-dependent mechanism. *Molecular pharmacology* 1997, 51 (5), 693–702. [PubMed: 9145907]
- 74). Berridge MJ The Inositol Trisphosphate/Calcium Signaling Pathway in Health and Disease. *Physiol. Rev.* 2016, 96 (4), 1261–96. [PubMed: 27512009]
- 75). Maxwell JT; Blatter LA A novel mechanism of tandem activation of ryanodine receptors by cytosolic and SR luminal Ca²⁺ during excitation-contraction coupling in atrial myocytes. *J. Physiol.* 2017, 595 (12), 3835–3845. [PubMed: 28028837]

- 76). Johny JP; Plank MJ; David T Importance of Altered Levels of SERCA, IP3R, and RyR in Vascular Smooth Muscle Cell. *Biophys. J.* 2017, 112 (2), 265–287. [PubMed: 28122214]
- 77). Adasme T; Haeger P; Paula-Lima AC; Espinoza I; Casas-Alarcon MM; Carrasco MA; Hidalgo C Involvement of ryanodine receptors in neurotrophin-induced hippocampal synaptic plasticity and spatial memory formation. *Proc. Natl. Acad. Sci. U. S. A.* 2011, 108 (7), 3029–34. [PubMed: 21282625]
- 78). Wolff MS; Fischbein A; Selikoff IJ Changes in PCB serum concentrations among capacitor manufacturing workers. *Environ. Res.* 1992, 59 (1), 202–16. [PubMed: 1425510]
- 79). Jursa S; Chovancova J; Petrik J; Loksa J Dioxin-like and non-dioxin-like PCBs in human serum of Slovak population. *Chemosphere* 2006, 64 (4), 686–91. [PubMed: 16337987]
- 80). DeCaprio AP; Johnson GW; Tarbell AM; Carpenter DO; Chiarenzelli JR; Morse GS; Santiago-Rivera AL; Schymura MJ Akwesasne Task Force on the, E., Polychlorinated biphenyl (PCB) exposure assessment by multivariate statistical analysis of serum congener profiles in an adult Native American population. *Environ. Res.* 2005, 98 (3), 284–302. [PubMed: 15910784]
- 81). Wolff MS; Schechter A Accidental exposure of children to polychlorinated biphenyls. *Arch. Environ. Contam. Toxicol.* 1991, 20 (4), 449–53. [PubMed: 1906267]
- 82). Brown JF Determination of PCB Metabolic, Excretion, and Accumulation Rates for Use as Indicators of Biological Response and Relative Risk. *Environ. Sci. Technol.* 1994, 28 (13), 2295–305. [PubMed: 22176047]
- 83). Pessah IN; Cherednichenko G; Lein PJ Minding the calcium store: Ryanodine receptor activation as a convergent mechanism of PCB toxicity. *Pharmacol. Ther.* 2010, 125 (2), 260–85. [PubMed: 19931307]
- 84). Bennett DL; Bootman MD; Berridge MJ; Cheek TR Ca²⁺ entry into PC12 cells initiated by ryanodine receptors or inositol 1,4,5-trisphosphate receptors. *Biochem. J.* 1998, 329 (Pt 2), 349–57. [PubMed: 9425119]
- 85). Cao Z; Xu J; Hulsizer S; Cui Y; Dong Y; Pessah IN Influence of tetramethylenedisulfotetramine on synchronous calcium oscillations at distinct developmental stages of hippocampal neuronal cultures. *NeuroToxicology* 2017, 58, 11–22. [PubMed: 27984050]
- 86). Lesiak A; Zhu M; Chen H; Appleyard SM; Impey S; Lein PJ; Wayman GA The environmental neurotoxicant PCB 95 promotes synaptogenesis via ryanodine receptor-dependent miR132 upregulation. *J. Neurosci.* 2014, 34 (3), 717–25. [PubMed: 24431430]
- 87). Wong PW; Joy RM; Albertson TE; Schantz SL; Pessah IN Ortho-substituted 2,2',3,5',6-pentachlorobiphenyl (PCB 95) alters rat hippocampal ryanodine receptors and neuroplasticity in vitro: evidence for altered hippocampal function. *Neurotoxicology* 1997, 18 (2), 443–56. [PubMed: 9291493]
- 88). Schantz SL; Seo BW; Wong PW; Pessah IN Long-term effects of developmental exposure to 2,2',3,5',6-pentachlorobiphenyl (PCB 95) on locomotor activity, spatial learning and memory and brain ryanodine binding. *Neurotoxicology* 1997, 18 (2), 457–67. [PubMed: 9291494]
- 89). Kim KH; Pessah IN Perinatal exposure to environmental polychlorinated biphenyls sensitizes hippocampus to excitotoxicity ex vivo. *NeuroToxicology* 2011, 32 (6), 981–5. [PubMed: 21571002]

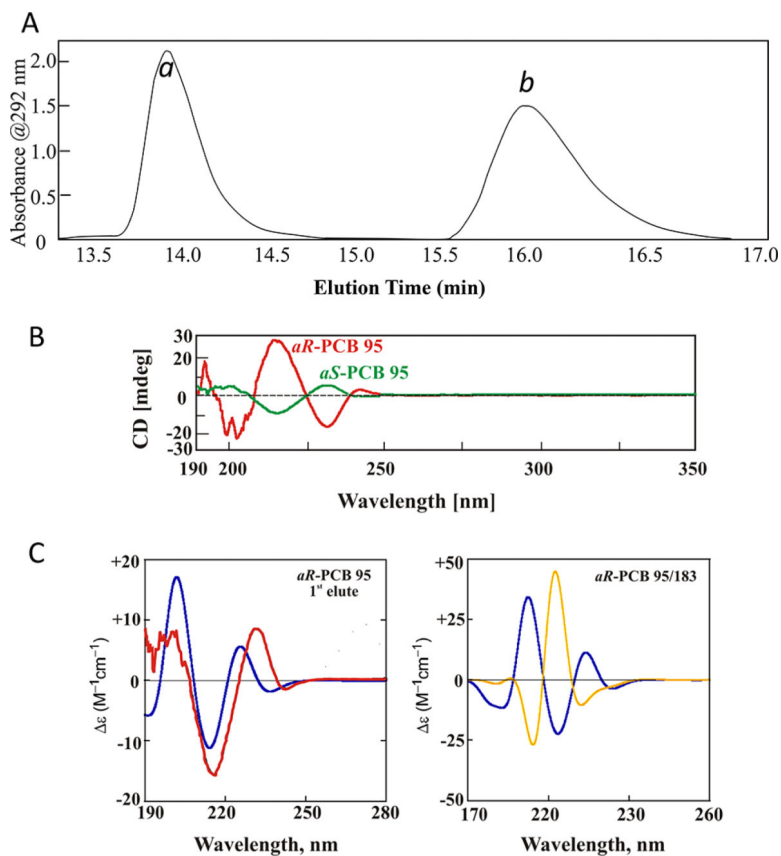


Figure 1. Separation of enantiomeric PCB 95. Panel A: Elution profile from three tandem chiral columns monitored at 292 nm (Panel A); Panel B: CD spectra for *aR*-PCB 95B and *aS*-PCB 95B; Panel C: Left graph: the theoretically predicted CD spectrum for *aR*-PCB-95B (Blue) together with experimental CD spectrum predicted for the first elute (Red) from chiral HPLC, allowing unambiguously assignment of the absolute configuration; right graph: comparison of theoretical CD spectra for PCB 95 (blue) and PCB 183 (yellow) with the same *aR* configuration. Note that the observed Cotton effects in the main bands are mostly opposite due to the reversal of the directions of transition dipole moments, while the signs of the first transitions are both negative.

RyR1-Enriched SR Membrane

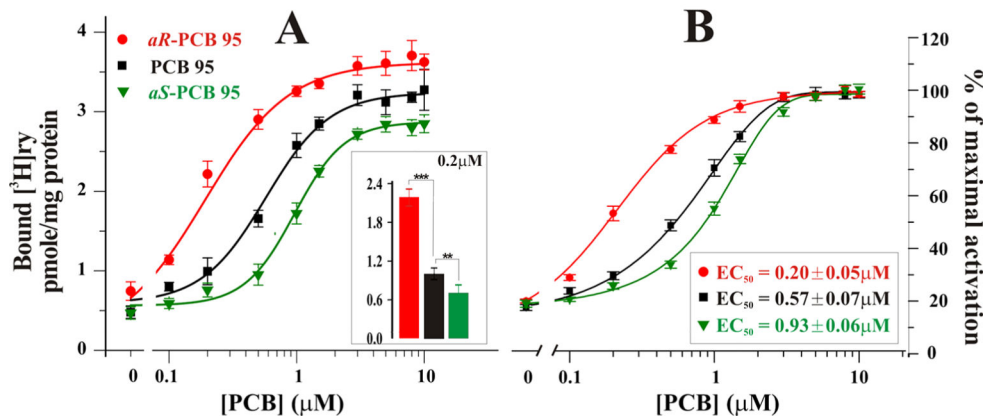


Figure 2.

Differentiated activation effects of enantiomeric PCB 95 on $[^3\text{H}]$ Ryanodine binding to RyR1-enriched SR membrane. Left panel (A) is the concentration-dependent activation of specific $[^3\text{H}]$ Ryanodine binding. The insert bar-graph is the specific bound $[^3\text{H}]$ Ry in the presence of $0.2 \mu\text{M}$ *aR*-PCB-95B (red), racemate (black) and *aS*-PCB-95B (green). Right panel (B) is the normalized specific binding (% of maximal activation) with obtained EC_{50} displayed in the inset. The presented data are mean \pm SD from two independent measurements of two different JSR preps ($n = 2$), each with quadruplet samples. Insert in Panel A, *** indicates the $p < 0.001$; ** $p < 0.01$ (One-way ANOVA followed by post hoc Dunnett's test was used to analyze the data at 95% confidence intervals).

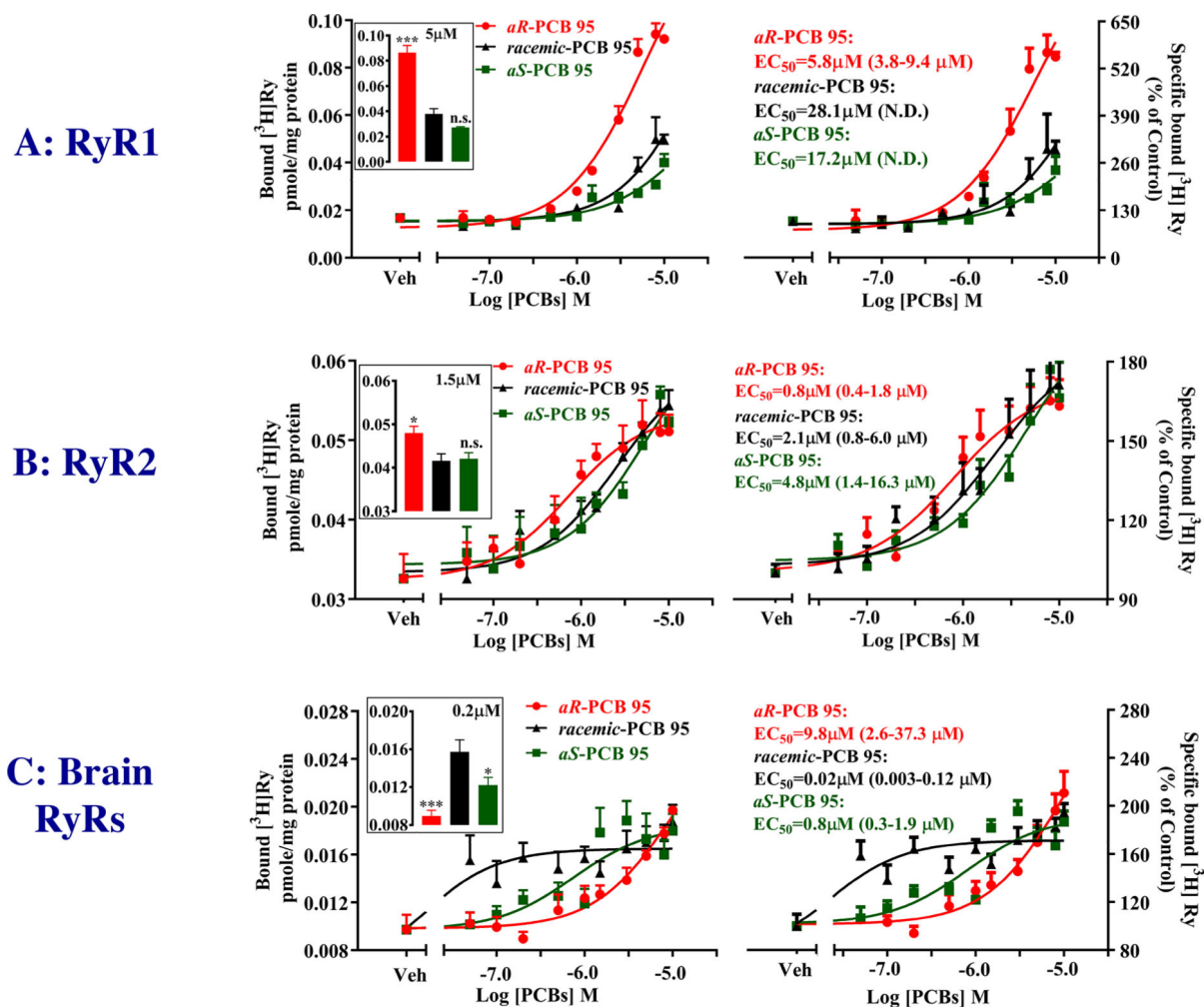


Figure 3.

Enantioselective actions of PCB 95 on three isoforms of RyR. Tissue homogenates were made from mouse skeletal muscle (RyR1; Panel A), heart (RyR2; Panel B) and brain cortex (Brain RyRs; Panel C). Data expressed as Mean \pm SEM and concentration response curves were assessed using three parameter nonlinear regression using Graph Pad 7.03. For each panel, the inserted bar graph in the left side shows the absolutely specific bound [3 H]Ry in the presence of 5, 1.5, and 0.2 μ M *aR*-PCB-95B (red), racemate (black) and *aS*-PCB-95B (green), respectively. On the right side of each panel is shown normalized specific bound [3 H]Ry (% of control) with generated EC₅₀ in the inset. Data points shown in the graphs from one assay ($n = 1$; Panel A), or two independent assays ($n = 2$; Panels B, $n = 2$; Panel C), respectively, with each assay conducted in triplicates. Data in inserted bar graph expressed as mean \pm SEM, $n = 3-6$. * $p < 0.05$, *** $p < 0.001$ vs racemate using One-way ANOVA followed by post hoc Dunnett's test. n.s. indicates no significance, N.D. means not detectable.

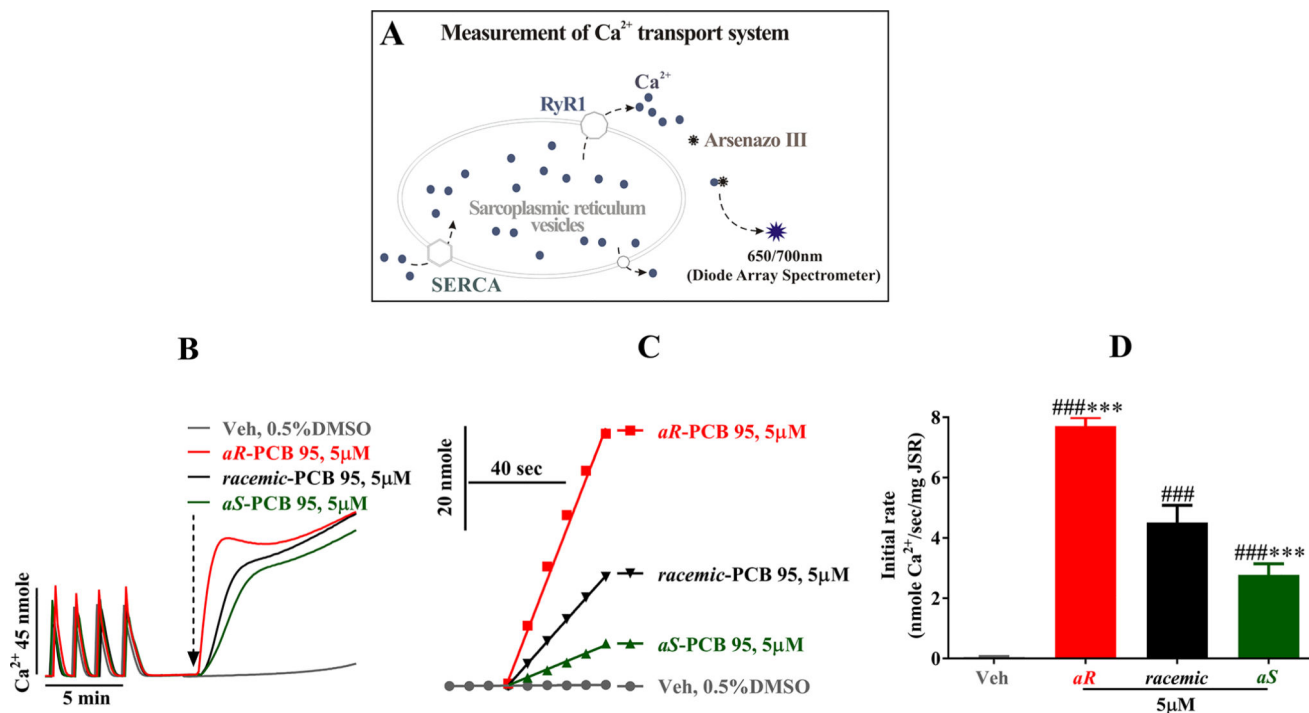


Figure 4. PCB 95 enantioselectively induce rapid Ca²⁺ release from JSR vesicles. The upper panel (Panel A) is the schematic illustration showing the Ca²⁺ transport system monitored with Ca²⁺ dye Arsenazo III. Panel B: JSR vesicles were actively loaded with four bouts of total 180 nmole Ca²⁺ before exposed to DMSO, enantiomeric or racemic PCB 95 (black) as marked in the figure. Panel C: The initial 60 s of Ca²⁺ release traces were presented with a linear-fit. The obtained initial release rates (nmole Ca²⁺/sec/mg) from total *n* = 6 independent measurements under identical condition were summarized and plotted in Panel D. Data presented as mean ± SD (*n* = 6). ### *p* < 0.001 vs vehicle (0.5% DMSO), ****p* < 0.001 vs racemic-PCB95 (One-way ANOVA followed by post hoc Dunnett’s test using Graphpad Prism 7.03).

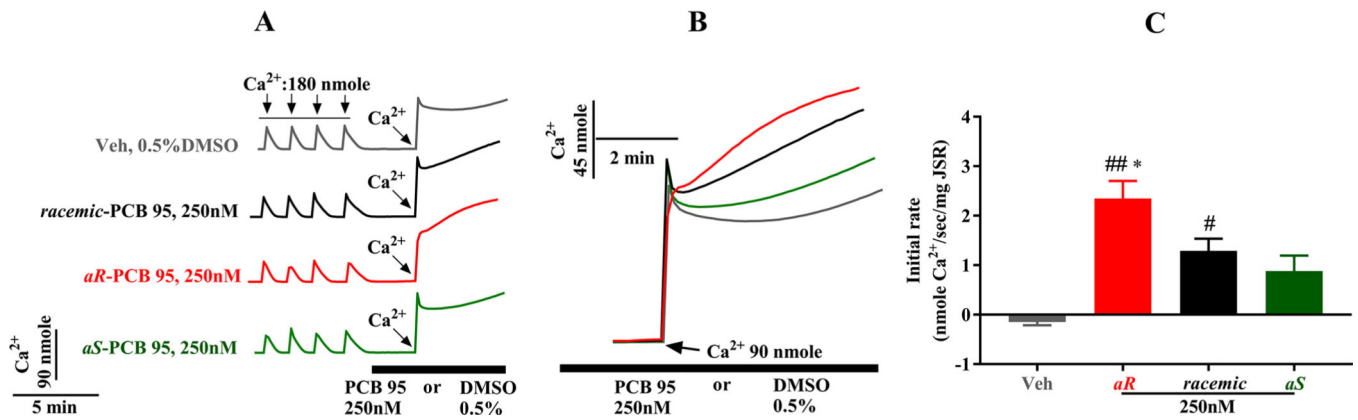
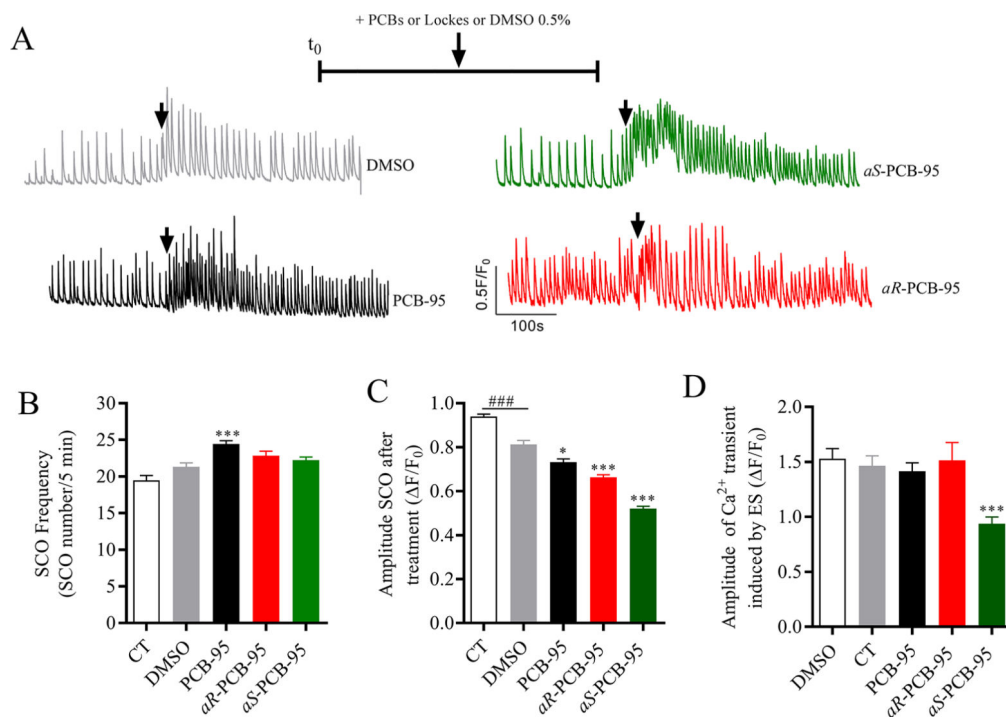


Figure 5.

Enantioselectively Potentiated Ca²⁺-induced Ca²⁺ release (CICR) by PCB 95. Ca²⁺ was actively loaded up to approximate 70% of the vesicles' loading capacity before exposed to DMSO (0.5%) or 250 nM PCB 95 (As shown by black bar). Actively loaded Ca²⁺ uptake and release were shown in panel A, panel B displayed the Ca²⁺ induced Ca²⁺ release in the absence (0.5% DMSO, Gray) /presence of 250 nM enantiomeric or racemic PCB 95 (Black). The initial 60 s of Ca²⁺-induced Ca²⁺ release traces were linear fitted and expressed in nmole Ca²⁺/sec/mg, and presented in the Panel C. Data presented as mean \pm SEM, $n = 3-4$. # $p < 0.05$, ## $p < 0.01$ vs Veh (0.5% DMSO), * $p < 0.05$ vs rac-PCB95 (unpaired t test were performed using Graphpad Prism 7.03).

**Figure 6.**

Transient Ca²⁺ dynamics in cultured murine hippocampal neuron acutely exposure to PCB 95. Spontaneous synchronized Ca²⁺ oscillations were measured on single hippocampal neurons during 10 min in order to obtain the basal level of oscillation and then, either PCB-95s (*rac*-PCB95, *aR*-PCB-95 or *aS*-PCB-95) or vehicle (0.5% DMSO) was added to the well. (Panel A) Representative traces of SCO recording in the soma of the neurons in basal stage and then, in response to the addition (black arrow) of PCB-95s (500 nM of racemic-PCB95, *aR*-PCB-95, or *aS*-PCB-95) or vehicle (0.5% DMSO). Panels B and C represent respectively, the mean SCO frequency and amplitude of the SCO measured over 5 min after the addition either PCB-95s (500 nM of *rac*-PCB95, $n = 20$, *aR*-PCB-95, $n = 22$ or *aS*-PCB-95, $n = 24$) or vehicle (0.5% DMSO, $n = 28$). Panel D shows the amplitude of the Ca²⁺ transient induced by an electrical stimulation of 20 Hz (ES) after 10 min of PCB-95s (500 nM of *rac*-PCB95, $n = 18$, *aR*-PCB-95, $n = 18$ or *aS*-PCB-95, $n = 24$) or vehicle (0.5% DMSO, $n = 28$) exposure in hippocampal neurons (14 DIV). Significance was determined using One-Way ANOVA followed by Tukey's multiple comparison. *, $p < 0.05$; ***, $p < 0.001$ compared to DMSO vehicle; ###, $p < 0.001$ compared to Control (CT) with Lockes' addition. Error bars indicate mean \pm SEM.

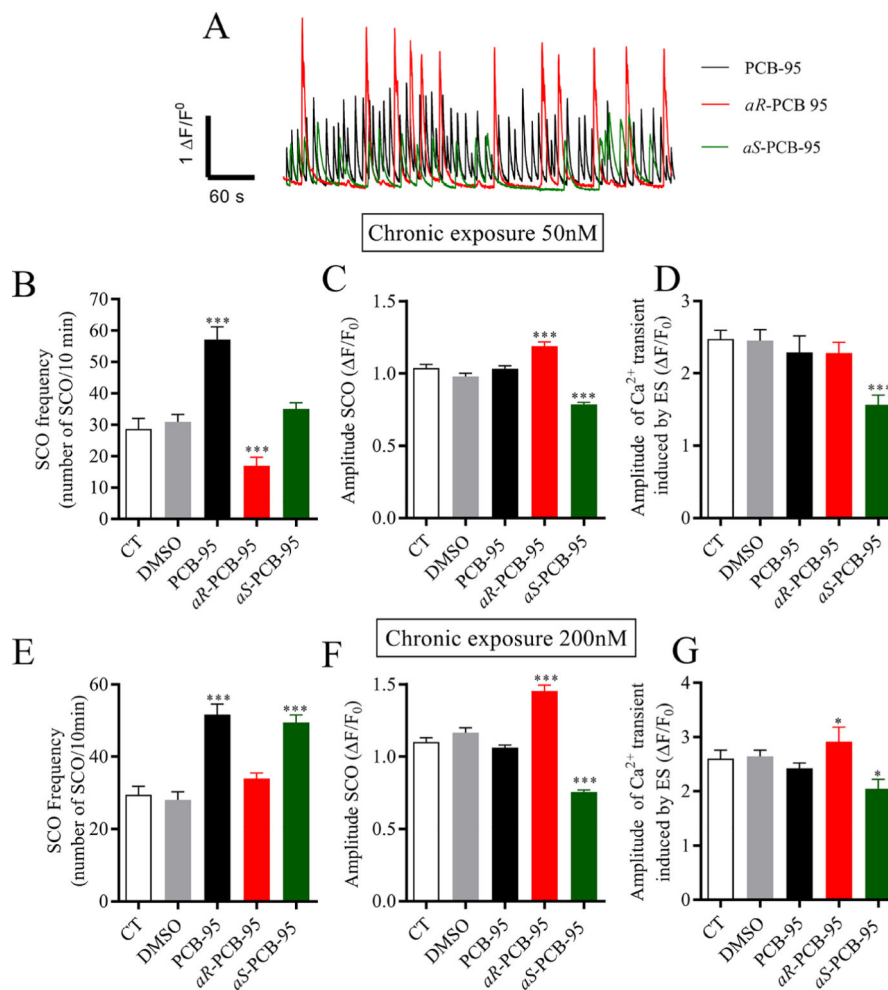


Figure 7.

Effects of chronic exposure of PCB-95 on synchronized Ca²⁺ oscillations (SCO) in cultured hippocampal neurons. Spontaneous synchronized Ca²⁺ oscillations were measured on single hippocampal neurons chronically exposed to 50 nM (upper panel, Panels A, B, C and D) and 200 nM (lower panel, Panels E, F, and G) of either PCB-95s (*rac*-PCB95, *aR*-PCB-95 or *aS*-PCB-95) or vehicle (0.2% DMSO) for 12 days. (Panel A) Representative traces of SCO recording in the soma of the treated hippocampal neurons with PCB-95s (500 nM of *rac*-PCB95, *aR*-PCB95, or *aS*-PCB-95). Panels B and C represent respectively, the mean SCO frequency and amplitude of the SCO measured over 10 min on chronically exposed neurons to either PCB-95s (50 nM of *rac*-PCB95, *n* = 10, *aR*-PCB-95, *n* = 25 or *aS*-PCB-95, *n* = 31) or vehicle (0.05% DMSO, *n* = 28). Panel D shows the amplitude of the Ca²⁺ transient induced by an electrical stimulation of 20 Hz (ES) after 10 min of basal SCO recording on chronically treated neurons with either PCB-95s (50 nM of *rac*-PCB95, *n* = 11, *aR*-PCB-95, *n* = 25 or *aS*-PCB-95, *n* = 32) or vehicle (0.05% DMSO, *n* = 25). Panels E and F represent respectively, the mean SCO frequency and amplitude of the SCO measured over 10 min on chronically exposed neurons to either PCB-95s (200 nM of *rac*-PCB95, *n* = 18, *aR*-PCB-95, *n* = 40 or *aS*-PCB-95, *n* = 49) or vehicle (0.2% DMSO, *n* = 45). Panel G shows the amplitude of the Ca²⁺ transient induced by an electrical stimulation of 20 Hz (ES) after 10 min of basal

SCO recording on chronically treated neurons with either PCB-95s (200 nM of *rac*-PCB95, $n = 14$, *aR*-PCB-95, $n = 19$ or *aS*-PCB-95, $n = 33$) or vehicle (0.2% DMSO, $n = 54$). Significance was determined using One-way ANOVA followed by Tukey's multiple comparison. *, $p < 0.05$; **, $p < 0.01$ compared to DMSO vehicle. Error bars indicate mean \pm SEM.

Author Manuscript

Author Manuscript

Author Manuscript

Author Manuscript